Fuel 387 (2025) 134348

Contents lists available at ScienceDirect

Fuel

journal homepage: www.elsevier.com/locate/fuel

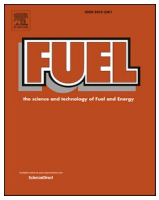

Short communication

Direct microscopic imaging of exploding aluminum/nitrocellulose mesoparticles to reveal the enhanced combustion mechanism

Yuxin Zhou, Keren Shi, Mahbub Chowdhury, Erik Hagen, Yujie Wang, Michael R. Zachariah *

Departments of Chemical Engineering and Materials Science, University of California, Riverside, CA 92521, United States

ARTICLE INFO

Keywords:
Aluminum
Nitrocellulose
Mesoparticles
Nanoenergetics

ABSTRACT

Aluminum/nitrocellulose (Al/NC) mesoparticles, assembled from nanoparticle components by spray-drying have previously been shown to have enhanced reactivity relative to Al nanoparticle aggregates, despite being significantly larger. The assembly approach is based on the premise of the NC acting as a gas generator to disperse the fuel nanoparticles prior to their sintering/combustion. Here we demonstrate this premise by direct observation of individual particle burning with ~ μs and ~ μm precision, by a high-speed camera coupled to an intensifier and a microscope. During the combustion of Al/NC mesoparticles, smaller burning particles are scattered outward. Such "firework-like" trajectories occur due to the decomposition of NC, which generates gas to disassemble the Al particles within the mesoparticle, reducing sintering and promoting the oxidation. While the combustion of Al nanoaggregates exhibits isolated trajectories. Al/NC mesoparticles exhibit a ~60 % decrease in burn time compared to Al nanoaggregates due to "firework-like" explosion.

1. Introduction

Aluminum (Al) is widely used as an additive for propellant, explosives and pyrotechnics due to its high energy density [1–3]. More recently, Al nanoparticles have attracted increased attention due to their lower ignition temperature and higher reaction rate [3–5] compared to Al microparticles. However, the practical utilization of Al nanoparticles faces challenges. One of these is particle sintering [6–8], where nano-sized Al particles sinter into larger structures before or at the reaction front. Sintering characteristic times are typically much lower than reaction characteristic times [9], indicating that the rapid particle size increase could result in the loss of nanostructure and, consequently, the forfeiture of reactivity advantages. Quite a few methods have been explored in previous studies to mitigate the sintering issue, for instance, employing hollow carbon nanospheres [10] or carbon fibers [11–13] as prohibitors, or igniting with an ultrahigh heating rate [14]. Apart from the sintering issue, the addition of nano-sized Al particles into binder-based propellant formulation creates processing challenges which make the casting or printing more difficult [15].

One approach to mitigate some of these issues, is to integrate Al nanoparticles and gas-generating binders into mesoparticles with diameters on the scale of μm scale. This concept was first proposed and demonstrated by Wang et al. [16] by creating micron-scale particles from Al nanoparticles and nitrocellulose (NC). Subsequent studies incorporating oxidizer nanoparticles showed enhanced thermite reactivity [17]. Jacob et al. [18] employed electrospray assembly to manufacture mesoparticles composed of Al nanoparticles and NC and demonstrated the enhanced reactivity of Al/NC mesoparticles compared to Al nanoparticles in lab-scale flames; while similar phenomena were also reported in the application of Al/NC mesoparticles in solid propellants [19]. The improvement was attributed to the early gas-releasing of NC, whose relatively low thermal decomposition temperature causes the Al nanoparticles previously assembled in mesoparticles to disperse prior to ignition and thus minimize sintering. Despite the demonstrated significant advantages, electrospray assembly is constrained by its low yield (typically in the magnitude of mg/h) [18], which poses a great challenge for its industrial scalability. Chowdhury et al. [20] employed spray-drying assembly to manufacture mesoparticles and found that spray-dried mesoparticles had a similar reactivity compared to mesoparticles made by electrospray, but with a much higher yield (in the magnitude of g/h). In this work, we assemble Al and NC to mesoparticles by spray drying and combust them in temperature-controlled exhaust hot gas of fuel-lean methane/oxygen/nitrogen quasi-premixed flames. *In-operando* microscopic imaging is utilized to observe the burning characteristics of Al/NC mesoparticles. It is the first time to have a direct insight into Al/NC mesoparticle exploding process, and pivotal for

* Corresponding author.
E-mail address: mrz@engr.ucr.edu (M.R. Zachariah).

https://doi.org/10.1016/j.fuel.2025.134348
Received 31 May 2024; Received in revised form 13 December 2024; Accepted 6 January 2025
Available online 11 January 2025

understanding the combustion mechanism of mesoparticles.

2. Methods

The schematic of the burner (also commonly referred to as Hencken burner) is presented in Fig. 1(a), and a more detailed description can be found in our previous studies [18,21]. The burner chamber is filled with stainless steel balls, with multiple tubes inserted into it. The mixture of methane and nitrogen comes through the tubes. While oxygen is delivered through the gaps between the tubes and stainless-steel balls, providing a uniform laminar outlet velocity, resulting in a quasi-premixed flame above the burner. For the purposes of this study, the burner is employed to produce a homogenous temperature field of hot gas, into which particles are injected. At the center of the burner is a tube (~1 mm ID) through which particles are carried by nitrogen and injected into the flames. Before injection, particles are loaded into a sealed chamber which is connected to a nitrogen carrier gas supply. After injection, the aerosolized particles are of sufficient low density that the burning behavior of each particle can be regarded as individual. This is demonstrated by the microscopic imaging in Section 3. A total of four post-flame environments are investigated in this work and their flame conditions are summarized in Table S1 and S2 of Supplementary data. They are all fuel-lean methane/oxygen/nitrogen flames, providing oxygen-rich post-flame region, but have different equivalence ratios and consequently have different adiabatic flame temperatures. The flow rates of methane, oxygen, nitrogen for generating flame and nitrogen for carrying particles are metered with four MKS mass flow controllers. The equivalence ratios φ of the four flames are 0.25, 0.3, 0.35 and 0.4 respectively. The adiabatic temperatures calculated by Chemkin-Pro [22] using the thermodynamic data of USC Mech II [23] are 1823, 2030, 2200 and 2338 K respectively. Temperature distributions along with the flame height in post-flame regions are measured by the rapid insertion of B-type thermocouple (OMEGA) with radiation heat loss correction [24–27] and the results are presented in Fig. 1(c). Thermocouple measurement is detailed in the Supplementary data. With this configuration flame temperature decreases with increasing height above the burner. The maximum flame temperature (near the burner surface) is difficult to measure by thermocouple, so the calculated adiabatic flame temperature is used as an upper limit estimation.

To directly observe the burning trajectories of individual particles in flames, a high-speed camera (Vision Research Phantom VEO710L) coupled with a long working distance microscope objective (Infinity Photo-Optical Model K2 DistaMax), and a high-speed intensifier (Lambert HiCATT 25) are employed. Based on calibration, the imaging system has a resolution of ~1.7 μm/pixel and all measurement are taken at a vertical height of ~3 cm above the burner surface.

Imaging of the entire flame is also conducted with a high-speed camera (Vision Research Phantom Miro M110) coupled with a macro lens (Nikon), primarily for the estimation of particle burn time.

The spray-drying synthesis methodology of Al/NC mesoparticles has been comprehensively discussed in our previous research [20], thus only a brief description is presented here. First, solid NC is dissolved in a 3:4:3 (volume ratio) N, N-dimethylformamide (DMF): *iso*-propanol (IPA): acetone mixture; then Al nanoparticles (100 nm, US Research Nanomaterials) is added to the mixture to form a suspension. For safety reasons, the solid loading in Al/NC precursor suspension is low (10 mg/mL). Then, the suspension is stirred for ~ 12 hrs and sonicated for ~ 1 hr. Finally, the suspension is atomized with a BÜCHI B-290 Mini spray dryer at a feed rate of ~ 12.5 L/min. Preheated argon at ~ 110 °C is used as the drying gas with an inlet flow rate of ~ 360 L/min throughout the spray drying process. The resultant particle internal structure is shown in Fig. 1(b). DMF, IPA and acetone evaporate from the droplets, to generate Al/NC mesoparticles which are collected by a cyclone-based collector. The weight percentage of NC in Al/NC mesoparticles is 7.5 %, which has been demonstrated in our previous study [20] to be sufficient for effectively dispersing the particles within the mesoparticle

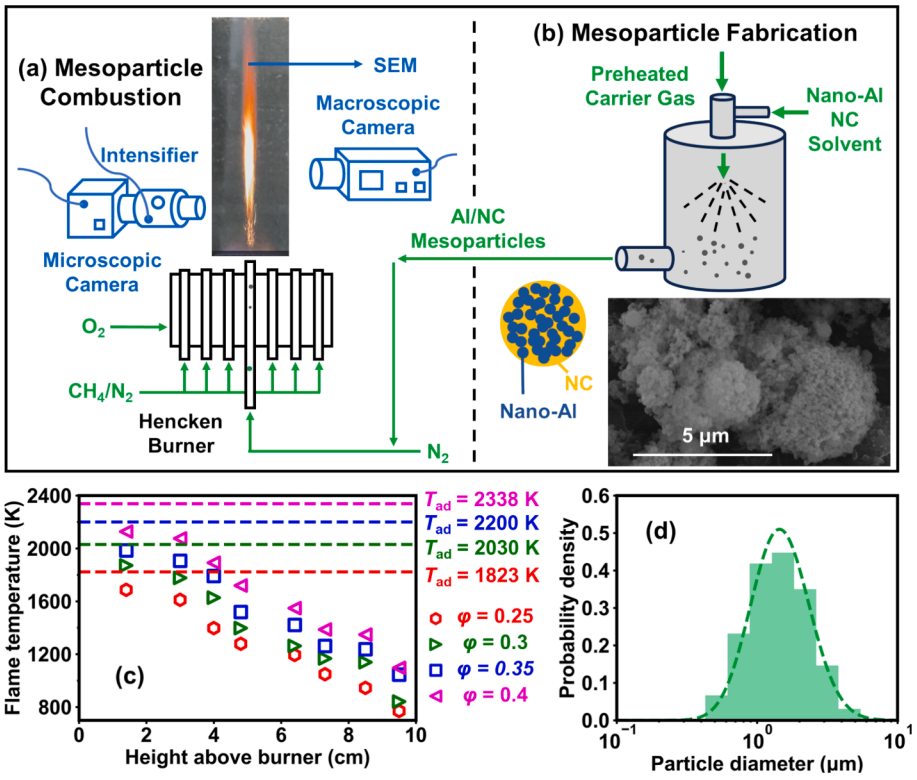

Fig. 1. (a) Diagram of Hencken burner and the diagnostics; (b) Al/NC mesoparticle spray-drying synthesis methodology, SEM image and the internal structure diagram of Al/NC mesoparticle; (c) Measured methane/oxygen/nitrogen quasi-premixed flame temperature distribution (without any particles); (d) Particle size distribution of spray dried Al/NC mesoparticles (histogram represents experimental data and dashed line represents fitted function).

during combustion. The morphology and elemental distribution of Al/NC mesoparticles is observed by scanning electron microscopy (SEM, FEI Nova NanoSEM 450) coupled with energy dispersive X-ray spectroscopy (EDS). A representative SEM image is shown in Fig. 1(b), and the distribution of particle sizes is shown in Fig. 1(d). Although the diameter of mesoparticles is generally in the μm scale, we can still clearly distinguish the outlines of nanoparticles within the mesoparticle. EDS mapping results demonstrate that the distribution of Al in Al/NC mesoparticles is very uniform. Additional SEM images and EDS maps are presented in Supplementary data.

Commercial Al nanoparticles (100 nm) and microparticles (10 μm) from US Research Nanomaterials are employed to compare with spray-dried Al/NC mesoparticles. Nascent Al nanoparticles are included in this study because Al/NC mesoparticles are an assembly of these nanoparticles; Al microparticles are included for comparison because the diameter of Al/NC mesoparticles are on the μm scale. Although Al nanoparticles have an average primary particle size in the nm scale, they tend to heavily aggregated. Hence, it is more accurate to refer to them as Al nanoaggregates hereafter. More details about all the materials introduced in this paragraph are presented in Supplementary data.

3. Results and discussion

The combination of high-speed camera, microscopic objective and intensifier enables the *in-operando* observation on the burning characteristics of individual Al/NC mesoparticles as well as Al nanoaggregates. As the enhancement of intensifier is not uniform across different wavelengths, all intensified images are converted to grayscale to avoid color misinterpretation. Fig. 2 shows some representative microscopic images, captured by the high-speed camera operating at a sampling rate of 19,000 fps, with the intensifier in "always-on" state. It should be noted that a larger number of particle movements are not precisely situated on the focal plane, hence their trajectories appear blurred or even cannot be captured.

The most important observation and the motivating reason for this work is the unambiguous result that mesoparticles dissemble; some mesoparticles split into 2–3 parts, as shown in the right two subfigures in Fig. 2(a); while others undergo more violent disintegrations, releasing numerous burning particles, forming "firework-like" trajectories, as shown in the left three subfigures in Fig. 2(a). In contrast, the burning of Al nanoaggregates only has isolated, and almost linear-shaped luminous trails. No scattering trajectories can be observed. As for Al microparticles, no burning trajectories can be observed because they cannot be ignited within the temperature range we investigate.

The results in Fig. 2 are from an intensifier in the "always-on" state, which shows streaks due to the framing rate limits in the high-speed camera. However, if the intensifier is configured to operate as a fast shutter, then motion can be captured as show in Fig. 3. In this case, the resolution and focus position are unchanged, however the sampling rate of high-speed camera is only 1000 fps, with an exposure time of 1 ms, but the electronic shutter frequency of intensifier is set as 100 kHz, with a gate of 1 μs, leading to 100 images per camera frame. We can see more clearly in Fig. 3(a), the explosions of mesoparticles. Some of them just split into two parts, as shown in the rightmost subfigure of Fig. 3(a) and some of them explode to numerous pieces, as shown in the left two subfigures of Fig. 3(a). While no signs of the disintegration of Al nanoaggregates can be observed, since their burning trajectories are almost perfect individual dotted lines, as shown in Fig. 3(b).

The velocities of particles can also be calculated by counting the dots per frame. Not surprisingly, and despite the explosions, the velocities of exploding Al/NC mesoparticles and Al nanoaggregates essentially at the linear gas velocity (~10 m/s), since the characteristic relaxation time in this size range is very short (~10 μs). Although the particles can be ejected from the mesoparticles due to outgassing, they would quickly be relaxed to the local gas velocity because of the drag force.

More microscopic images on exploding Al/NC mesoparticles can be found in Figs. S3 and S4 in the Supplemental.

The "firework-like" trajectories of Al/NC mesoparticles burning suggest the breakdown of mesoparticles before combustion, as shown in Fig. 4. The thermal decomposition temperature of NC increases with heating rate, from ~475 K at 5 K/min in thermogravimetric analysis (TGA) [28] to ~575 K at 1.3×10^5 K/s in temperature-jump mass spectrometry [29]. Although measuring the heating rate of particles in the flame is beyond the scope of this study, it is undoubtedly

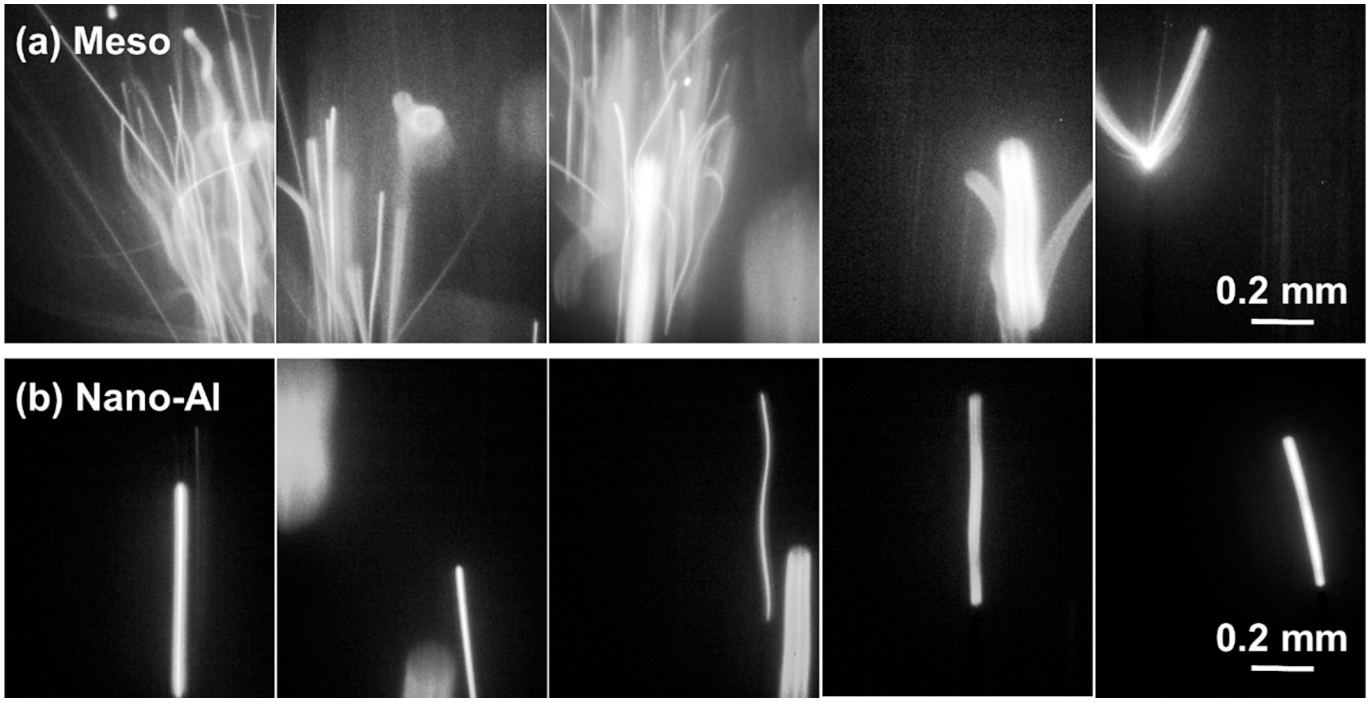

Fig. 2. Microscopic grayscale images of the combustion of (a) Al/NC mesoparticles and (b) Al nanoaggregates sampled at 19,000 fps (exposure time of camera: 50 μs, intensifier in a "always-on" state).

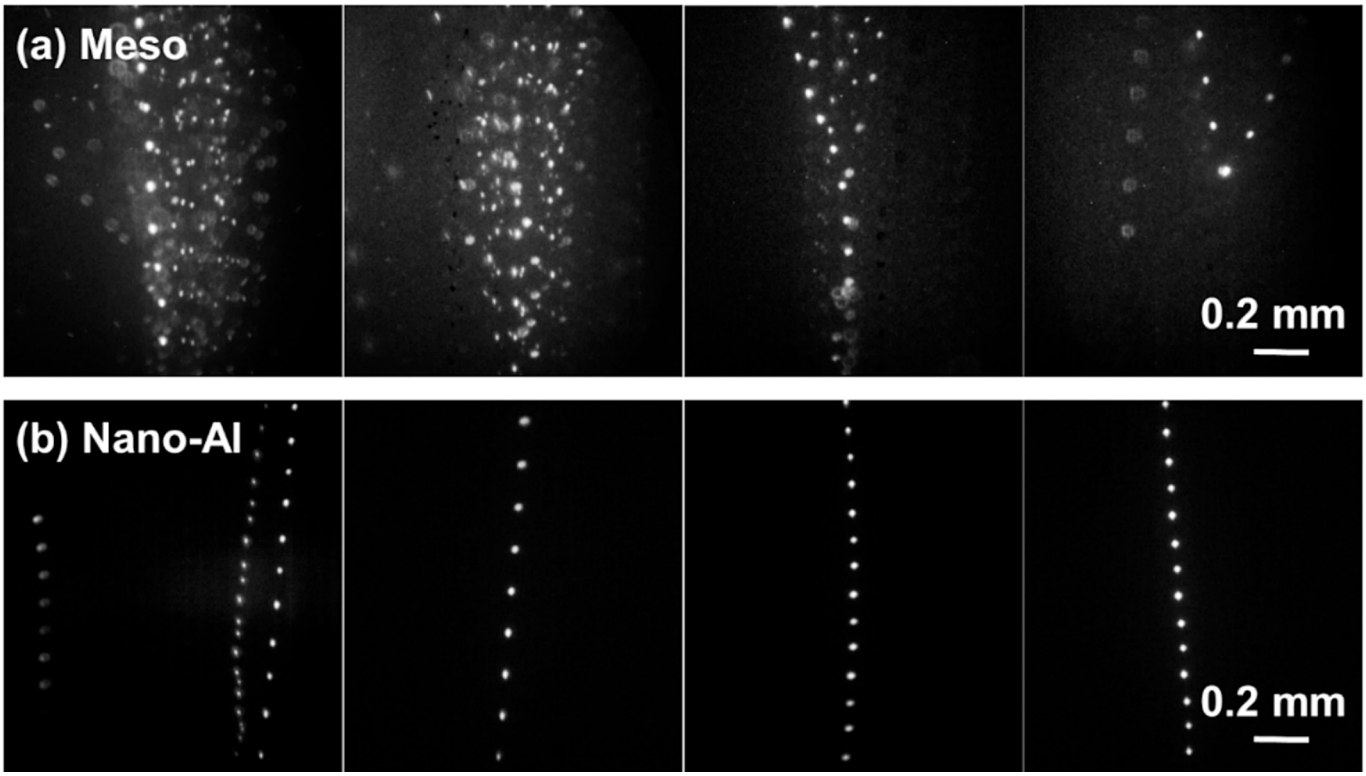

Fig. 3. Microscopic grayscale images of the combustion of (a) Al/NC mesoparticles and (b) Al nanoaggregates sampled at 1000 fps (exposure time of camera: 1 ms, intensifier gate time: 1 μs, intensifier frequency: 100 kHz).

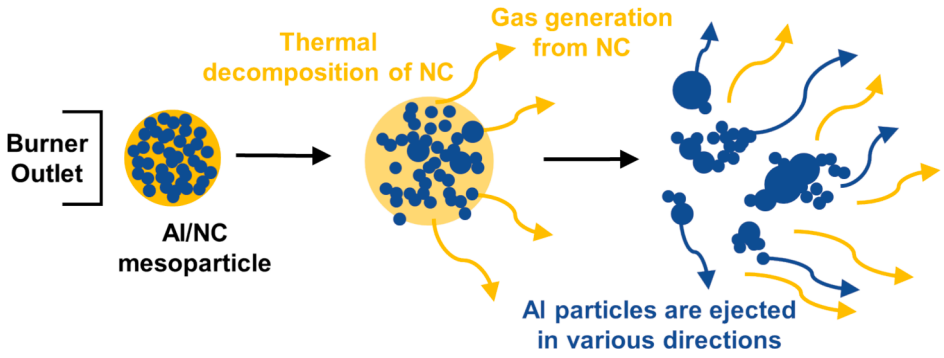

Fig. 4. Mechanism for the enhanced combustion of Al/NC mesoparticles.

significantly higher than that of a TGA, suggesting a decomposition temperature close to 575 K. Thus, when Al/NC mesoparticles are dissembled by NO, NO_2, CO, CH_2O, CO_2, etc. from NC decomposition [29], this should primarily occur before Al ignition since Al nanoparticle ignition is typically about 1000 K. It also implies that at the point of NC decomposition, the temperature of Al/NC mesoparticle should be very close to the flame temperature. The material density of NC is ~ 1 g/cm^3 [30], while the densities of small molecular weight gases from the decomposition of NC are generally on the order of magnitude of ~ 10^{-3} g/cm^3, making them thousands of times less dense than solid NC. This means that 7.5 wt% NC in mesoparticles can produce enough gas to disperse the particles to a volume hundreds of times larger than that of the initial mesoparticles.

Compared to the chemical modification method of Al nanoparticles by surface functionalization [31] or coating [32,33], Al/NC mesoparticle is a physical strategy based on the gas generation from NC. This outgassing process can effectively mitigate the sintering of Al particles, pushing them away from each other, forming the "firework-like" trajectories, as shown in Fig. 2(a) and 3(a). Combustion after exploding is surely enhanced due to the higher specific surface area of particles and less diffusion distance for surrounding oxygen.

Despite having primary particle sizes in nm scale, Al nanoparticles are heavily aggregated (Fig. S1). Once these nanoaggregates are ejected into flames, they are prone to severe sintering, thereby diminishing their kinetic advantages as nanoparticles. They can hardly be dispersed to the surroundings like Al/NC mesoparticles, and thus only have isolated burning trajectories shown in Fig. 2(b) and 3(b).

Fig. 5(a-d) presents the typical macroscopic images of Al/NC mesoparticles, Al nanoaggregates, and Al microparticles in flames, with their sampling rates and gains (G) indicated. Their scales and focus locations are similar but not the same because of the separate experiments. It is clear that most of Al microparticles are not ignited at all, since luminescent trajectories can hardly be observed. The burning trajectories of Al nanoaggregates show a few isolated luminescent lines, which is consistent with microscopic images. The burning characteristics of Al/NC mesoparticles differs significantly from that of Al nanoaggregates,

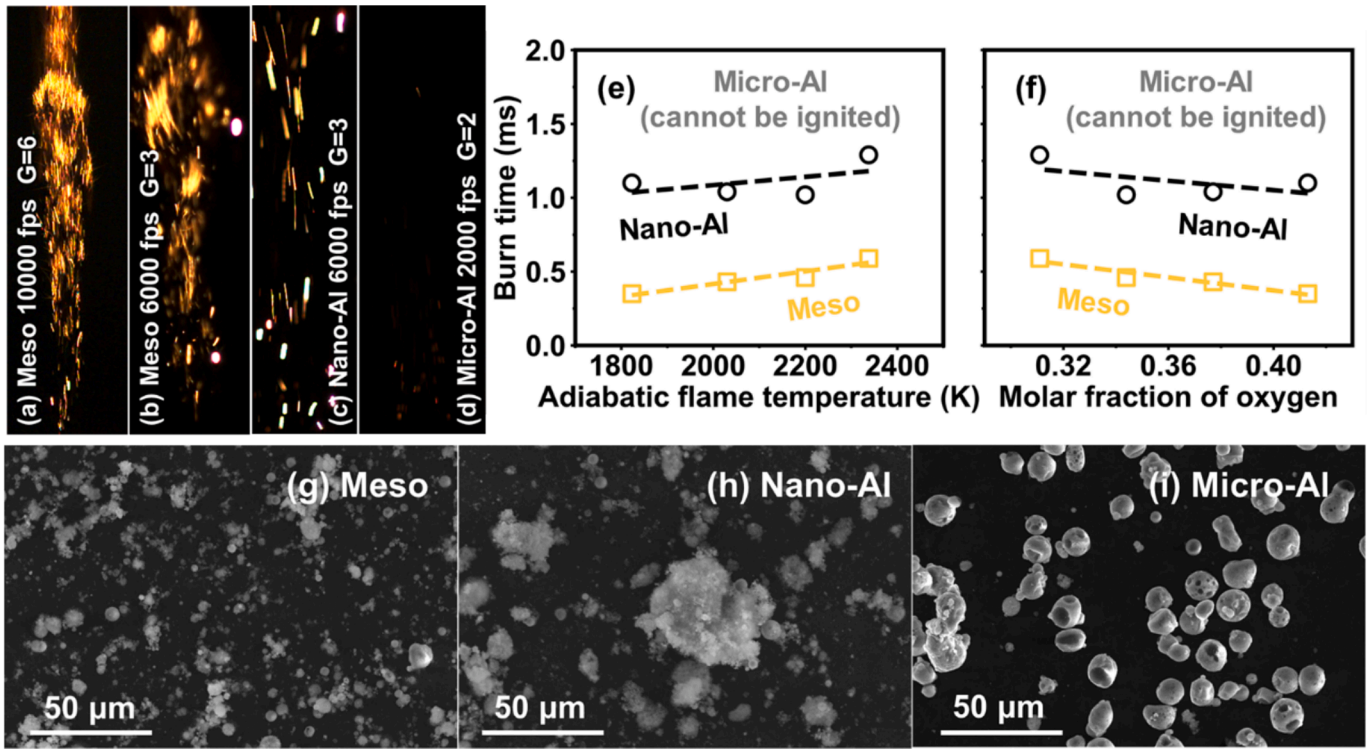

Fig. 5. Macroscopic images of Al/NC mesoparticles (a-b), Al nanoaggregates (c) and Al microparticles (d) in flames; burn time of the aforementioned three types of particles under different flame conditions (e-f); SEM images of post-combustion products of the aforementioned three types of particles (g-i).

even when observed from a macroscopic perspective. At lower sampling rates (6000 fps), the burning of Al/NC mesoparticles appears "cloud-like". When the sampling rate is elevated to 10,000 fps and the gain is doubled, it becomes apparent that the "cloud" consists of the numerous burning Al particles released from the explosion of Al/NC mesoparticles, which is consistent with microscopic images.

Since the macroscopic high-speed videos on the particle burning in flames have been obtained, it is straightforward to estimate the burn time. Considering that the brightness of burning Al particle markedly surpasses the methane flame background, burn time can be determined by tracing the luminous burning trajectories frame by frame and then multiplying the total number of frames by the interval time. For each set of flame conditions, 80 burning trajectories are documented for each particle type. Fig. 5 (e-f) illustrates the calculated average burn time of three types of particles, at four different flame conditions. In general, the average burn time shows very slight dependency on flame conditions. For Al nanoaggregates, their average burn time is ~ 1.11 ms, which is consistent to the "burn time – particle size" relationship map concluded by Sundaram et al. [3] as well as Huang et al. [5] For Al/NC mesoparticles, their average burn time is only ~ 0.46 ms, which is very similar to the results by Jacob et al. [18] on Al/NC mesoparticles synthesized by electrospray. Average burn time of Al/NC mesoparticles is lower than that of Al nanoaggregates by ~ 60 %. The Al nanoparticles used for synthesizing Al/NC mesoparticles are the same as the Al nanoaggregates for burning directly, which means their thermal properties and reactivity are the same. Therefore, the enhanced reactivity of Al/NC mesoparticles should be primarily attributed to mesoparticle exploding. For Al microparticles, their average burn time cannot be calculated because most of them are not ignited in all four flame conditions.

The post-combustion products are also characterized. A piece of carbon tape, attached to the pin stub designed for SEM specimen, is swiped quickly across the flame several times at the height of ~ 10 cm above the burner. Post-combustion products deposit on the carbon tape via thermophoresis, can be observed by SEM. Some representative images are shown in Fig. 5(g-i) and more images can be found in Fig. S5 of Supporting Information. The ignition of Al microparticles relies on the melting of the oxide shell, and thus has a much higher ignition temperature (~2350 K) compared to that of Al nanoparticles (~1000 K) [3]. Given that the adiabatic flame temperature in this work ranges from 1823 to 2338 K, it is not surprising that Al microparticles fail to ignite. The morphology of Al microparticles is almost unchanged before and after the ejection into flames, exhibiting a highly uniform particle size distribution centered at ~10 μm. For Al/NC mesoparticles, although they also have an average particle size in μm scale initially, they explode into small components, that do not sinter as much, leading to smaller post-combustion product sizes. For Al nanoaggregates, we observe larger post-combustion product, in some cases, up to ~50 μm. The particle size distributions of these post-combustion products are presented in the Supplementary data. The average volume of post-combustion product of Al nanoaggregates is 8x that of Al/NC mesoparticles. Thus, *ex situ* SEM images align with *in-operando* microscopic imaging, i.e., Al/NC mesoparticles explode into smaller particles, enhancing combustion rate.

4. Conclusion

In summary, high speed intensified microscopy is employed to image the explosion process of Al/NC mesoparticles and the validation of our conceptual model for how these structures behave.

A high-speed intensifier, a long working distance microscope objective as well as a high-speed camera are combined to achieve high spatial (~μs) and temporal (~μm) resolution for *in-operando* imaging of the explosion process of Al/NC mesoparticles. These experiments more directly explain why Al/NC mesoparticles, despite their micron size, can burn faster that Al nanoparticle aggregates. *In-operando* microscopic images show that the burning of Al/NC mesoparticles exbibits "fire-work-like" luminous trajectories, indicating that numerous smaller Al particles are released from the breakdown of mesoparticles and pushed to the surroundings; while the burning of Al nanoaggregates only

exhibits a few isolated luminous trajectories. Al microparticles cannot be ignited in temperature range investigated in this paper. Since the thermal decomposition of NC occurs prior to the ignition of Al, the gas released from NC can disperse the Al particles previously assembled in mesoparticles, enabling them to burn with less sintering compared to Al nanoaggregates. Mitigated sintering is also confirmed by SEM images of post-combustion products.

CRediT authorship contribution statement

Yuxin Zhou: Writing – original draft, Formal analysis, Data curation. **Keren Shi:** Data curation. **Mahbub Chowdhury:** Data curation. **Erik Hagen:** Data curation. **Yujie Wang:** Data curation. **Michael R. Zachariah:** Writing – review & editing, Supervision, Resources, Project administration, Methodology, Investigation, Funding acquisition, Conceptualization.

Declaration of competing interest

The authors declare that they have no known competing financial interests or personal relationships that could have appeared to influence the work reported in this paper.

Acknowledgement

This work was supported by DTRA and ONR.

Appendix A. Supplementary data

Supplementary data to this article can be found online at https://doi.org/10.1016/j.fuel.2025.134348.

Data availability

Data will be made available on request.

References

[1] Dreizin EL. Metal-based reactive nanomaterials. Prog Energy Combust Sci 2009;35:141–67. https://doi.org/10.1016/j.pecs.2008.09.001.
[2] Ohkura Y, Rao PM, Zheng X. Flash ignition of Al nanoparticles: mechanism and applications. Combust Flame 2011;158:2544–8. https://doi.org/10.1016/j.combustflame.2011.05.012.
[3] Sundaram DS, Puri P, Yang V. A general theory of ignition and combustion of nano- and micron-sized aluminum particles. Combust Flame 2016;169:94–109. https://doi.org/10.1016/j.combustflame.2016.04.005.
[4] Wang J, Qu Y, Gong F, Shen J, Zhang L. A promising strategy to obtain high energy output and combustion properties by self-activation of nano-Al. Combust Flame 2019;204:220–6. https://doi.org/10.1016/j.combustflame.2019.03.016.
[5] Huang Y, Risha GA, Yang V, Yetter RA. Combustion of bimodal nano/micron-sized aluminum particle dust in air. Proc Combust Inst 2007;31:2001–9. https://doi.org/10.1016/j.proci.2006.08.103.
[6] Chu Q, Chang X, Chen D. A physiochemical model for the combustion of aluminum nano-agglomerates in high-speed flows. Combust Flame 2022;237:111739. https://doi.org/10.1016/j.combustflame.2021.111739.
[7] Raut JS, Bhagat RB, Fichthorn KA. Sintering of aluminum nanoparticles: a molecular dynamics study. Nanostructured Mater 1998;10:837–51. https://doi.org/10.1016/S0965-9773(98)00120-2.
[8] Wang H, Kline DJ, Zachariah MR. In-operando high-speed microscopy and thermometry of reaction propagation and sintering in a nanocomposite. Nat Commun 2019;10:3032. https://doi.org/10.1038/s41467-019-10843-4.
[9] Chakraborty P, Zachariah MR. Do nanoenergetic particles remain nano-sized during combustion? Combust Flame 2014;161:1408–16. https://doi.org/10.1016/j.combustflame.2013.10.017.
[10] Yang H, Xu C, Man S, Bao H, Xie Y, Li X, et al. Effects of hollow carbon nanospheres on combustion performance of Al/Fe2O3-based nanothermite sticks. J Alloys Compd 2022;918:165684. https://doi.org/10.1016/j.jallcom.2022.165684.
[11] Wang H, Hagen E, Shi K, Herrera S, Xu F, Zachariah MR. Carbon fibers as additives to engineer agglomeration and propagation of aluminized propellants. Chem Eng J 2023;460:141653. https://doi.org/10.1016/j.cej.2023.141653.
[12] Wang H, Kline DJ, Rehwoldt MC, Zachariah MR. Carbon fibers enhance the propagation of high loading nanothermites: in situ observation of microscopic combustion. ACS Appl Mater Interfaces 2021;13:30504–11. https://doi.org/10.1021/acsami.1c02911.
[13] Zhou Y, Zachariah MR. Molecular dynamics study on the capture of aluminum particles by carbon fibers during the propagation of aluminum-based energetics. Energy Fuels 2024;38:8992–9000. https://doi.org/10.1021/acs.energyfuels.4c00832.
[14] Monk I, Schoenitz M, Dreizin EL. The effect of heating rate on combustion of fully dense nanocomposite thermite particles. Combust Sci Technol 2018;190:203–21. https://doi.org/10.1080/00102202.2017.1380002.
[15] Wang H, Shen J, Kline DJ, Eckman N, Agrawal NR, Wu T, et al. Direct writing of a 90 wt% particle loading nanothermite. Adv Mater 2019;31:1806575. https://doi.org/10.1002/adma.201806575.
[16] Wang H, Jian G, Yan S, DeLisio JB, Huang C, Zachariah MR. Electrospray formation of gelled nano-aluminum microspheres with superior reactivity. ACS Appl Mater Interfaces 2013;5:6797–801. https://doi.org/10.1021/am401238t.
[17] Wang H, Jian G, Egan GC, Zachariah MR. Assembly and reactive properties of Al/CuO based nanothermite microparticles. Combust Flame 2014;161:2203–8. https://doi.org/10.1016/j.combustflame.2014.02.003.
[18] Jacob RJ, Wei B, Zachariah MR. Quantifying the enhanced combustion characteristics of electrospray assembled aluminum mesoparticles. Combust Flame 2016;167:472–80. https://doi.org/10.1016/j.combustflame.2015.09.032.
[19] Young G, Wang H, Zachariah MR. Application of nano-aluminum/nitrocellulose mesoparticles in composite solid rocket propellants. Propellants Explos Pyrotech 2015;40:413–8. https://doi.org/10.1002/prep.201500020.
[20] Chowdhury M, Ghildiyal P, Rojas A, Wang Y, Wang H, Zachariah MR. High-yield spray drying assembly and reactive properties of nanoenergetic mesoparticle composites. Adv Powder Technol 2023;34:104075. https://doi.org/10.1016/j.apt.2023.104075.
[21] Zong Y, Jacob RJ, Li S, Zachariah MR. Size resolved high temperature oxidation kinetics of nano-sized titanium and zirconium particles. J Phys Chem A 2015;119:6171–8. https://doi.org/10.1021/acs.jpca.5b02590.
[22] ANSYS Chemkin-Pro Software. https://www.ansys.com/products/fluids/ansys-chemkin-pro.
[23] Wang H, You X, Joshi AV, Davis SG, Laskin A, Egolfopoulos F, Law CK. USC Mech Version II. High-Temperature Combustion Reaction Model of H2/CO/C1-C4 Compounds; May 2007. http://ignis.usc.edu/USC_Mech_II.htm.
[24] Zhou Y, He Q, Sha Y, Shen C, You X. Effects of ferrocene addition on soot formation characteristics in laminar premixed burner-stabilized stagnation ethylene flames. J Aerosol Sci 2024;175:106265. https://doi.org/10.1016/j.jaerosci.2023.106265.
[25] Zhou Y, Wang M, He Q, You X. Experimental investigation on the size-dependent maturity of soot particles in laminar premixed ethylene burner-stabilized stagnation flames. Proc Combust Inst 2023;39:1147–55. https://doi.org/10.1016/j.proci.2022.09.030.
[26] Tang Y, Zou X, Dong W, Shi B, Wang N, Li S. Temperature measurements and high-speed photography of micron-sized aluminum particles burning in methane flat-flame exhaust. Fuel 2021;306:121743. https://doi.org/10.1016/j.fuel.2021.121743.
[27] Camacho J, Liu C, Gu C, Lin H, Huang Z, Tang Q, et al. Mobility size and mass of nascent soot particles in a benchmark premixed ethylene flame. Combust Flame 2015;162:3810–22. https://doi.org/10.1016/j.combustflame.2015.07.018.
[28] Pourmortazavi SM, Hosseini SG, Rahimi-Nasrabadi M, Hajimirsadeghi SS, Momenian H. Effect of nitrate content on thermal decomposition of nitrocellulose. J Hazard Mater 2009;162:1141–4. https://doi.org/10.1016/j.jhazmat.2008.05.161.
[29] Zhou L, Piekiel N, Chowdhury S, Zachariah MR. T-Jump/time-of-flight mass spectrometry for time-resolved analysis of energetic materials. Rapid Commun Mass Spectrom 2009;23:194–202. https://doi.org/10.1002/rcm.3815.
[30] French DM. The density of cellulose nitrate. J Appl Polym Sci 1978;22:309–13. https://doi.org/10.1002/app.1978.070220123.
[31] Jiang Y, Wang Y, Baek J, Wang H, Gottfried JL, Wu C-C, et al. Ignition and combustion of Perfluoroalkyl-functionalized aluminum nanoparticles and nanothermite. Combust Flame 2022;242:112170. https://doi.org/10.1016/j.combustflame.2022.112170.
[32] Ao W, Gao Y, Zhou S, Li LKB, He W, Liu P, et al. Enhancing the stability and combustion of a nanofluid fuel with polydopamine-coated aluminum nanoparticles. Chem Eng J 2021;418:129527. https://doi.org/10.1016/j.cej.2021.129527.
[33] Li Y, Chen Y, Cui W, Tang W, Wang B, Han Z. Preparation of Al/Ni Nano-composite Particles via Replacement Reaction and Their Characterization. ChemistrySelect 2020;5:13673–7. https://doi.org/10.1002/slct.202003350.